Physics and Imaging in Radiation Oncology 22 (2022) 57–62

Contents lists available at ScienceDirect

Physics and Imaging in Radiation Oncology

journal homepage: www.sciencedirect.com/journal/physics-and-imaging-in-radiation-oncology

# Intrafraction target shift comparison using two breath-hold systems in lung stereotactic body radiotherapy

Alejandro Prado [a,*], Daniel Zucca [a], Miguel Ángel De la Casa [a], Jaime Martí [a], Leyre Alonso [a], Paz García de Acilu [b], Juan García [b], Ovidio Hernando [d], Pedro Fernández-Letón [a,b], Carmen Rubio [c,d]

[a] Medical Physics and Radiation Protection Department, HU HM Sanchinarro, HM Hospitales, c\ Oña n°10, 28050 Madrid, Spain
[b] Medical Physics and Radiation Protection Department, HU HM Puerta del Sur, HM Hospitales, Av. Carlos V n° 70, 28938 Móstoles, Madrid, Spain
[c] Radiation Oncology Department, HU HM Sanchinarro, HM Hospitales, c\ Oña n°10, 28050 Madrid, Spain
[d] Radiation Oncology Department, HU HM Puerta del Sur, HM Hospitales, Av. Carlos V n° 70, 28938 Móstoles, Madrid, Spain

ARTICLE INFO

*Keywords:*
Stereotactic Body Radiotherapy
Respiratory motion management
Deep inspiration breath-hold
Intrafraction motion estimation
Surface-guidance system
Spirometry-based system

ABSTRACT

*Background and purpose:* In lung Stereotactic Body Radiotherapy (SBRT) respiratory management is used to reduce target motion due to respiration. This study aimed (1) to estimate intrafraction shifts through a Cone Beam Computed Tomography (CBCT) acquired during the first treatment arc when deep inspiration breath-hold (DIBH) was performed using spirometry-based (SB) or surface-guidance (SG) systems and (2) to analyze the obtained results depending on lesion localization.

*Material and methods:* A sample of 157 patients with 243 lesions was analyzed. A total of 860 and 410 fractions were treated using SB and SG. Averaged intrafraction shifts were estimated by the offsets obtained when registering a CBCT acquired during the first treatment arc with the planning CT. Offsets were recorded in superior-inferior (SI), left–right (LR) and anterior-posterior (AP). Significance tests were applied to account for differences in average offsets and variances between DIBH systems. Systematic and random errors were computed.

*Results:* Average offset moduli were $2.4 \pm 2.2$ mm and $3.5 \pm 2.6$ mm for SB and SG treatments ($p < 0.001$). When comparing SB and SG offset distributions in each direction no differences were found in average values ($p > 0.3$). However, variances were statistically smaller for SB than for SG ($p < 0.001$). The number of vector moduli offsets greater than 5 mm was 2.1 times higher for SG. Compared to other locations, lower lobe lesions moduli were at least 2.3 times higher.

*Conclusions:* Both systems were accuracy-equivalent but not precision-equivalent systems. Furthermore, the SB system was more precise than the SG one. Despite DIBH, patients with lower lobe lesions had larger offsets than superior lobe ones, mainly in SI.

## 1. Introduction

In Stereotactic Body Radiation Therapy (SBRT), high doses in a reduced number of fractions are imparted to the target [1]. Hence, steep dose gradients must be achieved to spare as much normal tissue as possible. Respiratory motion is one of the major uncertainty sources in lung treatments [2]. The current practice to account for respiratory motion uncertainties is to increase Planning Target Volume (PTV) margins, thus ensuring the prescribed dose delivery [3]. However, the volume of normal tissue is increased, which might increase the risk of radiation-related toxicity [4,5]. Dose delivery accuracy can be augmented by the use of respiratory management techniques such as abdominal compression [6], 4-dimensional Computed Tomography (4DCT) [7], Deep Inspiration Breath-Hold (DIBH) [8] and real-time tumor tracking [9,10].

Through the introduction of DIBH for lung SBRT, the patients might benefit from two effects: (1) the mitigation of the respiratory motion that might lead to PTV margins reduction [11] and (2) lung inflation, which decreases both irradiated lung volume and potential side effects [11]. Moreover, DIBH also reduces interplay effect, improves plan

* Corresponding author at: Hospital Universitario HM Sanchinarro, HM Hospitales, c\ Oña n°10, 28050 Madrid, Spain.
*E-mail addresses:* alejandropb_@hotmail.com, aprado@hmhospitales.com (A. Prado).

https://doi.org/10.1016/j.phro.2022.04.004
Received 22 September 2021; Received in revised form 13 April 2022; Accepted 20 April 2022

robustness [8] and enhance Cone Beam Computed Tomography (CBCT) image quality compared to free breathing [12].

Several studies have reported the feasibility, reproducibility and compliance of DIBH treatments [13–15]. DIBH can be performed using a spirometer-based system (SB) that measures the breathing volume [11,14,16,17], an optical surface tracking systems with external markers [9], an infrared tracking block [18] or a surface-guidance systems (SG) [8,19]. DIBH is considered a reliable and effective technique to reduce highly-moving target motion, such as lung lesions in free breathing conditions [8].

The election of the motion management system would affect intra- and inter-fractional errors and PTV margins that should be applied [3]. With the introduction of daily CBCT, imaging with soft-tissue registration the inter-fractional uncertainties can be reduced [12,16,20,21]. Regarding DIBH intrafraction shift estimations several methodologies have been reported: differences between CBCTs acquired before and after treatment delivery [16,19,22,23] and shifts obtained when registering the planning CT and an intrafraction CBCT performed during a treatment arc [20,24]. A more detailed estimation is shown by real-time tumor monitoring methods [9,10,25,26], which provide a complete picture of the intrafraction motion of lung lesions. By using DIBH intrafraction motion is mitigated, but not completely eradicated [9]. The main causes might be the imperfect breath-hold reproducibility [27] and the influence of heartbeat on tumor motion [25,26].

Lung tumor motion in free-breathing conditions has been addressed by several authors [25,28]. However, the number of studies when DIBH lung SBRT was performed is still low, as well as the number of patients included [20,27,29]. Furthermore, a comparison of intrafraction shifts estimated with the same procedure when using SB or SG systems to perform lung SBRT has not been published yet.

The purpose of this work was (1) to estimate intrafraction shifts through a CBCT acquired during the first treatment arc when DIBH was performed using SB or SG systems and (2) to analyze intrafraction shift results depending on lesion localization.

## 2. Material and methods

### 2.1. Patient selection

From January 2018 to June 2021, 157 patients with lung lesions treated with SBRT were retrospectively analyzed. The number of targets per patient ranged from 1 to 5, and a total of 243 lesions were treated using daily image guidance (CBCT). For each lesion one isocenter was utilized. From this sample, 78 lesions corresponding to 55 patients were treated using Catalyst-DIBH (CRAD, AB Sweden), which is a SG system. The remaining 165 lesions, related to 102 patients, were treated employing the Active Breathing Coordinator (Elekta, AB Sweden), which is a SB system. A total of 1270 DIBH treatment fractions were analyzed. Local approval was granted for this work and written informed consent was obtained from all patients.

### 2.2. Simulation and DIBH procedures

Both patient groups were simulated in supine position, with their arms abducted above the head. A BlueBag BodyFix evacuated cushion (Elekta AB, Sweden) adapted to patient anatomy along with a C-Qual Breastboard (Civco Radiotherapy, USA) were utilized for immobilization purposes for both SB and SG patients. For every patient a CT scan with a 2 mm slice separation was performed using a Toshiba Aquilion CT (Canon Medical Systems, Japan).

For SB treatments patients were required to use a mouthpiece connected to a spirometer, which measured the volume of air inhaled. Patients were trained to perform a DIBH for at least 20 s. The volume of air inhaled was recorded and the threshold value was adjusted to 80% of maximum inhaled volume. By means of goggles, the patients were instructed to perform a DIBH to exceed the threshold level. Once exceeded the air flow was cut and the patients were not able to inhale or exhale until they stopped pressing a control switch.

For SG treatments, a region of the patient's surface located under the xiphoid was selected to monitor the respiratory cycle. Once this region was located, the respiratory base line (BL) was extracted from the free-breathing pattern. With the aid of goggles, the patient was able to visualize its own respiratory cycle and was instructed to perform a DIBH for at least 20 s. A 4 mm gating window (GW) was employed and the BL-GW distance was adapted to ensure patient's comfort during treatment. The BL-GW distance was kept constant through the entire treatment for every patient.

For both patient groups only one CT in DIBH conditions was acquired.

### 2.3. Planning and treatment.

Patients were prescribed 60 Gy in 3 or 5 fractions. At least 95% of the PTV should be covered by the prescription dose while no more than 120% of the prescribed dose was allowed. Treatment plans were calculated in RayStation 10B (RaySearch, AB Sweden) with the collapsed cone algorithm using a 2 mm grid size. Treatments were delivered in a Versa HD linac (Elekta AB, Sweden) with a flattening-filter-free (FFF) 6 MV energy photon beam. The treatment beam arrangements were composed of two arcs with gantry angles ranging from 180.5° to 30° (right lobe) and from 179.5° to 330° (left lobe).

In the treatment room, the patients were aligned by using tattoos (SB treatments) or by means of surface guidance (SG treatments). During treatment, both patient groups used visual guidance by means of goggles. After patient alignment, a set-up CBCT was performed in DIBH to correct for patient positioning for both SB and SG treatments. To perform a full CBCT between 2 and 3 DIBHs were needed. Once the corrections were applied, the treatment started when the patient respiratory cycle exceeded the predefined threshold level associated with the amount of air inhaled (SB treatments) or it moved inside the GW (SG treatments). For both patient groups a second CBCT was acquired during the first treatment arc. The offsets obtained through this second CBCT were applied before the second treatment arc was delivered. From the offsets yielded by the second CBCT, an estimation of the averaged intrafraction shift [20,24] during the first treatment arc for each treatment fraction was obtained in superior-inferior (SI), left–right (LR) and anterior-posterior (AP) directions.

### 2.4. Set-up and intrafraction CBCT registrations

The registration procedure for both SB and SG patients was the same. The set-up CBCT was registered to the planning CT using soft tissue registration and focusing on the lesion. Only three-dimensional (3D) deviations from the planning CT were corrected. Regarding the CBCT acquired during the first treatment arc, the registration procedure was the same as for the set-up CBCT. Offsets were defined as the shifts obtained when registering the planning CT with the CBCT acquired during the first treatment arc.

### 2.5. Data analysis

A total of 860 and 410 fractions were analyzed for SB and SG treatments, respectively. The offsets obtained were recorded in SI, LR and AP directions. The vector modulus (M) was calculated. For each patient between 3 and 5 sets of data were obtained, depending on the number of fractions treated.

Average offsets, standard deviations ($\sigma_{STD}$), ranges and histograms were computed for both patient groups. Moreover, data were analyzed considering the full data set (FDS) and lesion localization: right upper lobe (RUL), right lower lobe (RLL), right middle lobe (RML), left upper lobe (LUL) and left lower lobe (LLL).

The percentage of offsets greater than 5 mm ($O_{>5}$) and 8 mm ($O_{>8}$)

were obtained for SB and SG treatments, as well as the percentage of offsets lower than 3 mm ($O_{<3}$). $O_{<3}$, $O_{>5}$ and $O_{>8}$ values were computed for each spatial direction and for M. Moreover, this analysis was performed for the FDS and for the five lesion locations.

For patients treated with SB and SG, respectively, systematic (Σ) and random (σ) errors were computed using the offsets obtained from the registration of the CBCT acquired during the first arc with the planning CT for every treatment fraction. Furthermore, these errors were obtained for each lesion localization and for the full data set (FDS). The methodology employed to calculate Σ and σ is described in van Herk [3].

To evaluate if differences in average offsets corresponding to distinct DIBH systems were significant a two-tailed Student *t*-test was employed. To account for significant differences in distribution variances a Fisher-Snedecor F-test was utilized. To properly use these tests normal distribution of the data were confirmed by Normal Q-Q plots. For the M distribution comparison, which was not normal, a Mann-Whitney *U* test was employed. P-values were recorded and a significance level of 0.01 was used after Bonferroni correction. R version 4.1.2 was employed for statistical analysis.

## 3. Results

Average offset values in SI, LR and AP directions for both FDS and lesion localization analyses were below 1.4 mm (Table 1). Differences between SB and SG average offsets were lower than 0.4 mm, except for 3 cases. P-values obtained from the Student *t*-test yielded that average offset differences were not significant when considering both FDS and lesion localization analyses (Table 2).

The widths of the distributions of offsets were wider for SG than for SB treatments (Fig. 1). Furthermore, standard deviations were higher for SG than for SB treatments for the same lesion localization and spatial direction considered (Table 1). The FDS Fischer-Snedecor F-test yielded p-values lower than 0.001 in the three spatial directions, which implied statistical significance. When lesion localization was accounted for, p-values were lower than 0.01 for right lobe lesions (SI, LR and AP), LUL lesions in AP and LLL lesions in LR (Table 2).

The FDS vector modulus analysis yielded 2.4 ± 2.2 mm and 3.5 ± 2.6 mm for SB and SG treatments, respectively (Table 1). The difference was 1.1 mm higher for SG than for SB treatments and p-values obtained were statistically significant (Table 2). Regarding lesion localization analysis, vector moduli were higher for SG than for SB treatments. However, the Mann-Whitney *U* test yielded significant p-values only for RUL and RLL lesions (Table 2). Data analysis showed that the largest shifts were not concentrated in the same patients but were randomly distributed between them.

Table 3 shows the offset percentage analysis. Considering the three directions and the FDS, $O_{<3}$ values were higher for SB than for SG treatments. The differences ranged from 3.5% (in LR) to 5% (in AP). Regarding vector moduli, the $O_{<3}$ value was 12% higher for SB than for SG treatments. When considering lesion localization for SB treatments $O_{<3}$ values were higher than for SG treatments except for RML lesions. These results were found in SI, LR, AP directions and for the vector modulus. Moreover, vector modulus $O_{<3}$ values were higher for upper lobe lesions than for lower lobe lesions.

For the FDS analysis $O_{>5}$ values were higher for SG treatments than for SB treatments in SI and AP directions (2.6% and 3.4% differences, respectively). For SG treatments vector modulus $O_{>5}$ value was 10% higher than for SB treatments. Regarding lesion localization, lower lobe lesions $O_{>5}$ values in SI were the highest for both SB and SG treatments. Moreover, the vector modulus $O_{>5}$ values were also the highest for lower lobe lesions.

For the FDS analysis $O_{>8}$ values were higher in SI for both SB and SG treatments. Lower lobe lesions $O_{>8}$ values in SI were the highest. The highest vector modulus $O_{>8}$ values were found for RLL lesions, which were 12.5% and 6.9% for SG and SB treatments, respectively.

Table 4 shows the systematic and random errors obtained. The Σ values were higher for SG treatments than for SB treatments considering both FDS and lesion localization analyses. However, Σ differences between DIBH systems were lower than 0.6 mm. The highest σ values were found for lower lobe lesions in SI and for SG treatments.

## 4. Discussion

In this study, we have shown that the averaged intrafraction shift

**Table 1**
Number of treatment fractions, average offsets, standard deviations ($\sigma_{STD}$) and ranges associated with the averaged intrafraction shifts estimated by a CBCT acquired during the first treatment arc when spirometry-based (SB) or surface-guidance (SG) systems were used to perform DIBH. Results were arranged by lesion localization and for the full data set. SI (superior-inferior), LR (left–right), AP (anterior-posterior), M (vector modulus), RUL (right upper lobe), RLL (right lower lobe), RML (right middle lobe), LUL (left upper lobe), LLL (left lower lobe) and FDS (full data set).

| | | SG | | | | SB | | | |
|---|---|---|---|---|---|---|---|---|---|
| Localization | Offset direction | # fractions | Average (mm) | $\sigma_{STD}$ (mm) | Range (mm) | # fractions | Average (mm) | $\sigma_{STD}$ (mm) | Range (mm) |
| RUL | SI | 125 | −0,4 | 2,2 | 13,0 | 206 | −0,8 | 1,6 | 10,0 |
| | LR | | 0,2 | 1,8 | 8,0 | | −0,2 | 1,1 | 9,0 |
| | AP | | −0,1 | 2,4 | 15,0 | | −0,5 | 1,4 | 10,0 |
| | M | | 3,1 | 2,1 | 9,5 | | 1,9 | 1,7 | 11,1 |
| RLL | SI | 84 | −0,5 | 4,5 | 27,0 | 209 | −1,0 | 2,7 | 5,0 |
| | LR | | 0,5 | 2,4 | 9,0 | | 0,1 | 1,4 | 10,0 |
| | AP | | −0,3 | 2,7 | 10,0 | | −0,3 | 1,5 | 12,0 |
| | M | | 4,8 | 3,3 | 17,3 | | 2,8 | 2,3 | 11,6 |
| RML | SI | 56 | −1,4 | 3,2 | 14,0 | 115 | −0,6 | 2,5 | 18,0 |
| | LR | | 0,0 | 1,3 | 5,0 | | −0,1 | 1,1 | 7,0 |
| | AP | | −0,5 | 1,3 | 6,0 | | −0,1 | 2,0 | 15,0 |
| | M | | 2,9 | 2,7 | 11,0 | | 2,5 | 2,3 | 13,2 |
| LUL | SI | 61 | −0,8 | 1,6 | 7,0 | 153 | −0,5 | 1,2 | 7,0 |
| | LR | | −0,2 | 1,6 | 9,0 | | 0,1 | 1,5 | 14,0 |
| | AP | | −0,4 | 2,4 | 15,0 | | −0,4 | 1,5 | 9,0 |
| | M | | 3,0 | 1,8 | 10,2 | | 2,1 | 1,5 | 9,3 |
| LLL | SI | 84 | −1,0 | 3,4 | 19,0 | 177 | −0,2 | 3,3 | 25,0 |
| | LR | | −0,4 | 1,7 | 11,0 | | −0,1 | 1,1 | 7,0 |
| | AP | | −0,4 | 2,1 | 10,0 | | −0,3 | 1,8 | 13,0 |
| | M | | 3,6 | 2,6 | 10,0 | | 2,8 | 2,7 | 14,4 |
| | SI | | −0,7 | 3,1 | 29,0 | | −0,6 | 2,4 | 25,0 |
| FDS | LR | 410 | 0,1 | 1,9 | 15,0 | 860 | 0,0 | 1,4 | 19,0 |
| | AP | | −0,2 | 2,4 | 16,0 | | −0,3 | 1,7 | 20,0 |
| | M | | 3,5 | 2,6 | 18,2 | | 2,4 | 2,2 | 14,4 |

**Table 2**
p-Values obtained from the comparison between spirometry-based (SB) and surface-guidance (SG) distribution average offsets (Student *t*-test) and variances (Fisher-Snedecor F-test) for each spatial direction. A Mann Whitney *U* test was employed for the comparison between SB and SG vector modulus distributions. Results were arranged by lesion localization and for the full data set. A significance level of 0.01 was utilized. SI (superior-inferior), LR (left–right), AP (anterior-posterior), M (vector modulus), RUL (right upper lobe), RLL (right lower lobe), RML (right middle lobe), LUL (left upper lobe), LLL (left lower lobe) and FDS (full data set).

| | Student T-test | | | Fischer-Snedecor F-test | | | Mann Whitney *U* test |
|---|---|---|---|---|---|---|---|
| Localization | SI | LR | AP | SI | LR | AP | M |
| RUL | 0,159 | 0,164 | 0,151 | ≪ 0,001* | ≪ 0,001* | ≪ 0,001* | ≪0,001* |
| RLL | 0,254 | 0,220 | 0,967 | ≪ 0,001* | ≪ 0,001* | ≪ 0,001* | ≪0,001* |
| RML | 0,206 | 0,899 | 0,394 | 0,043 | 0,171 | 0,017 | 0,511 |
| LUL | 0,134 | 0,407 | 0,800 | 0,018 | 0,311 | ≪ 0,001* | 0,011 |
| LLL | 0,125 | 0,144 | 0,662 | 0,288 | 0,001* | 0,111 | 0,047 |
| FDS | 0,709 | 0,297 | 0,492 | ≪ 0,001* | ≪ 0,001* | ≪ 0,001* | ≪ 0,001* |

* Statistically significant.

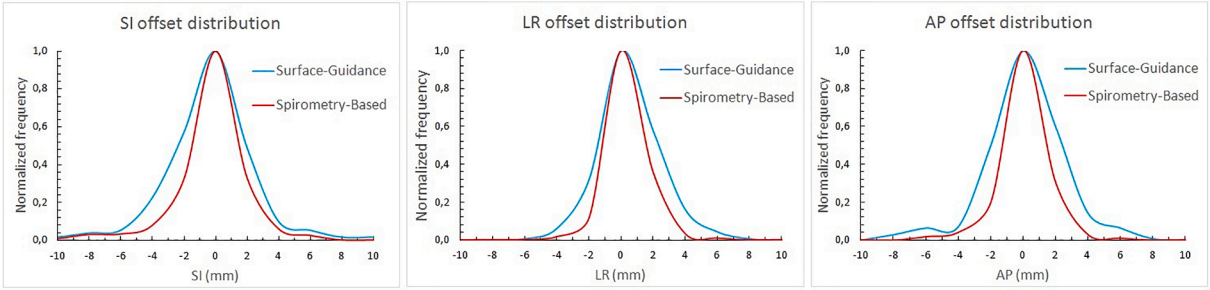


**Fig. 1.** Intrafraction offset distribution comparison between spirometry-based (SB) treatments (red), and surface-guidance (SG) treatments (blue), in superior-inferior (SI), left–right (LR) and anterior-posterior (AP) directions. The vertical axis represents the frequency and was normalized to 1.

estimated through a CBCT acquired during the first treatment arc was significantly higher for SG treatments, as yielded by the FDS vector modulus results. In addition, we have found that, for patients with right lobe lesions, vector moduli obtained were significantly higher for SG treatments. Moreover, intrafraction shifts were greater for patients with lower lobe lesions than for patients with upper lobe ones, mainly in SI.

The offset distribution analysis in SI, LR and AP directions showed that both DIBH systems could be considered as accuracy-equivalent, as averages were not statistically different when considering both FDS and lesion localization analyses. However, distribution widths (standard deviations) comparison yielded significant differences for the FDS analysis. Hence, SB was considered to be more precise than SG due to the smaller distribution widths obtained.

Wong YV et al. [9] studied tumor shifts based on a correlation model between external and internal markers for 14 patients. To perform DIBH authors utilized an SG system. The average shifts reported were 0.2 mm, 0.3 mm and 0.7 mm in LR, AP and SI, respectively. These results were quite similar to our average shift results for both SB and SG systems. In addition, their SI average results were at least two times higher than their AP and LR results, as well as we found. Lu et al. [29] studied GTV centroid shifts between three consecutive CTs performed using a SB system for 15 patients. Average shift reported were 2.9 mm, 0.6 mm and 1.5 mm, in SI, LR and AP directions, respectively. Their SI average offset was higher than both their LR and AP offsets, as we have obtained. However, their average shift results were higher than our values.

In den Otter et al. authors found that intrafraction motion was higher for inferior lobe lesions than superior lobe ones when using a SB system [30], which agreed with our SB and SG results.

Although DIBH clearly reduced lung tumor motion [8,11,31], intrafraction motion was still present [9,29]. Intrafraction tumor motion during DIBH might be dependent on the DIBH system used and might be caused by a quiet excursion of the diaphragm, an imperfect breath-hold or heartbeat influence.

RUL and RLL lesions might be less affected by the heartbeat due to their higher distance from the heart and the aortic arch. Hence, the influence of cardiac motion for right lobe lesions might be of less importance. However, RML lesions can be close to the heart. In Chen et al. [26] the authors showed that heartbeat influence was increased as overall tumor motion was decreased. In DIBH treatments, respiratory motion is reduced and the influence of heartbeat becomes more pronounced. Compared to SG, SB reduced the intrafraction shift. However, there were several cases for which distribution widths between SG and SB were not statistically distinct (Table 2). These results could be partially explained considering that heartbeat could influence SB treatments more. Tumor motion estimations due to heartbeat have been reported mainly in SI, but also in LR and AP [25,26]. Consequently, heartbeat might have increased SB distribution widths, moving them closer to SG ones. Therefore, F-tests yielded non-significant results (Table 2). Influence of heartbeat might be enhanced for RML lesions located near the heart. The presence of both heart and aortic arch near LUL lesions might also increase the SI and LR values [25]. Seppenwoolde et al. [25] investigated real-time intrafractional lung tumor motion using internal markers and fluoroscopy. The amplitude of tumor motion induced by heartbeat was addressed as well, being of 1–4 mm in LR and 1–2 mm in SI. These results might have been responsible for the increase in SB distribution widths, therefore inducing non-significant differences between SB and SG results for RML and LUL lesions (Table 2). LLL lesions are usually located at an inferior level than the heart. Hence, heartbeat influence in LR might be of less importance than in SI or AP. In Chen et al. the authors found that heartbeat influenced lung tumor motion in both SI and LR. This might explain the non-significant p-value obtained for LLL lesions when comparing SB and SG treatments in SI, but not in AP.

In Wang et al. [16], authors used a SB-system and reported systematic and random intrafraction errors obtained with two distinct methods: bony alignment and soft tissue registration. Σ ranged between 1 and 2 mm (SI), 0.9–1.1 (LR) and 1.8–1.9 mm (AP), and σ between 1.7 and 2.2 mm (SI), 1.5 (LR) and 2.9–4.1 mm (AP) for 19 patients. Our Σ results for SG and SB do concur (Table 4) with Wang et al. results. Regarding σ, AP values reported in Wang et al. were higher than ours for both systems. Our LR σ values were similar and our SI σ values were higher for SG, but similar for SB (Table 4). As interfractional errors in

**Table 3**
Percentages of offsets lower than 3 mm ($O_{<3}$) and>5 ($O_{>5}$) and 8 mm ($O_{>8}$), respectively. Values were presented for spirometry-based (SB) and surface-guidance (SG) treatments and were arranged by lesion localization and spatial direction. SI (superior-inferior), LR (left–right), AP (anterior-posterior), M (vector modulus), RUL (right upper lobe), RLL (right lower lobe), RML (right middle lobe), LUL (left upper lobe), LLL (left lower lobe) and FDS (full data set).

$O_{<3}$ (%)

| | SG | | | | SB | | | |
|---|---|---|---|---|---|---|---|---|
| | SI | LR | AP | M | SI | LR | AP | M |
| RUL | 91,4 | 96,2 | 91,4 | 72,4 | 95,2 | 98,8 | 95,2 | 83,7 |
| RLL | 78,1 | 89,1 | 89,1 | 45,3 | 83,4 | 94,9 | 96,0 | 65,1 |
| RML | 93,5 | 100,0 | 97,8 | 89,1 | 89,9 | 97,8 | 92,1 | 71,9 |
| LUL | 96,0 | 94,0 | 92,0 | 74,0 | 98,4 | 96,9 | 97,7 | 80,6 |
| LLL | 78,1 | 94,5 | 93,2 | 58,9 | 78,7 | 98,7 | 93,3 | 64,0 |
| FDS | 85,4 | 93,7 | 90,5 | 63,0 | 90,0 | 97,2 | 95,5 | 75,0 |

$O_{>5}$ (%)

| | SG | | | | SB | | | |
|---|---|---|---|---|---|---|---|---|
| | SI | LR | AP | M | SI | LR | AP | M |
| RUL | 1,9 | 0,0 | 4,8 | 11,4 | 2,4 | 0,6 | 1,2 | 4,2 |
| RLL | 12,5 | 0,0 | 7,8 | 26,6 | 7,4 | 0,6 | 0,6 | 13,7 |
| RML | 4,3 | 0,0 | 0,0 | 6,5 | 6,7 | 0,0 | 3,3 | 9,0 |
| LUL | 0,0 | 0,0 | 6,0 | 8,0 | 0,0 | 0,8 | 1,6 | 3,9 |
| LLL | 11,0 | 1,4 | 2,7 | 23,3 | 8,0 | 0,0 | 2,7 | 18,0 |
| FDS | 6,8 | 0,7 | 4,9 | 19,0 | 4,2 | 0,6 | 1,5 | 9,0 |

$O_{>8}$ (%)

| | SG | | | | SB | | | |
|---|---|---|---|---|---|---|---|---|
| | SI | LR | AP | M | SI | LR | AP | M |
| RUL | 0,0 | 0,0 | 1,9 | 5,7 | 0,0 | 0,0 | 0,0 | 1,2 |
| RLL | 6,3 | 0,0 | 0,0 | 12,5 | 2,9 | 0,0 | 0,0 | 6,9 |
| RML | 2,2 | 0,0 | 0,0 | 1,1 | 1,1 | 0,0 | 1,0 | 3,4 |
| LUL | 0,0 | 0,0 | 2,0 | 0,0 | 0,0 | 0,8 | 0,0 | 1,6 |
| LLL | 4,1 | 0,0 | 0,0 | 3,3 | 3,3 | 0,0 | 0,0 | 5,3 |
| FDS | 2,2 | 0,0 | 0,7 | 1,3 | 1,3 | 0,2 | 0,2 | 3,0 |

**Table 4**
Systematic (Σ) and random (σ) errors from spirometry-based (SB) and surface-guidance (SG) treatments associated with the averaged intrafraction shift estimated by a CBCT acquired during the first treatment arc. Data were arranged by lesion localization and spatial direction. SI (superior-inferior), LR (left–right), AP (anterior-posterior), RUL (right upper lobe), RLL (right lower lobe), RML (right middle lobe), LUL (left upper lobe), LLL (left lower lobe) and FDS (full data set).

Σ (mm)

| | | RUL | RLL | RML | LUL | LLL | FDS |
|---|---|---|---|---|---|---|---|
| SG | SI | 1,2 | 2,3 | 1,8 | 1,2 | 1,7 | 1,8 |
| | LR | 1,2 | 0,9 | 0,8 | 1,0 | 0,7 | 1,1 |
| | AP | 1,1 | 1,5 | 0,7 | 0,9 | 1,2 | 1,3 |
| SB | SI | 1,2 | 2,0 | 1,5 | 0,8 | 1,6 | 1,5 |
| | LR | 0,6 | 0,9 | 0,6 | 1,1 | 0,5 | 0,9 |
| | AP | 0,8 | 1,0 | 1,3 | 1,0 | 1,1 | 1,0 |

σ (mm)

| | | RUL | RLL | RML | LUL | LLL | FDS |
|---|---|---|---|---|---|---|---|
| SG | SI | 2,1 | 4,7 | 3,0 | 1,4 | 3,8 | 3,1 |
| | LR | 1,6 | 2,8 | 1,4 | 1,4 | 1,8 | 1,9 |
| | AP | 2,3 | 2,4 | 1,8 | 2,6 | 2,2 | 2,2 |
| SB | SI | 1,3 | 2,2 | 2,1 | 1,1 | 3,2 | 2,1 |
| | LR | 1,0 | 1,3 | 1,1 | 1,4 | 1,1 | 1,3 |
| | AP | 1,3 | 1,4 | 1,8 | 1,3 | 1,6 | 1,5 |

lung SBRT should be corrected by the use of daily IGRT, intrafraction Σ and σ should be used to calculate PTV margins instead. In this sense, each center should be responsible to study their uncertainties based on their intrafraction shift estimation procedures and DIBH systems utilized, as a similar analysis using different DIBH systems or intrafraction shift estimation methods might not result in similar findings.

In this study, the number of sessions analyzed has been higher compared to similar publications on lung tumor motion [20,32,33]. Consequently, a lesion localization analysis with a sufficient number of fractions per localization has been possible. The majority of studies addressing intrafractional lung motion in DIBH conditions utilize SB systems [16,17,27,29]. Nevertheless, this is the first study in which SB and SG systems are compared using as intrafraction shift estimation procedure a CBCT acquired during treatment arcs.

Regarding the limitations of our study, it is worth mentioning that the intrafraction shift estimation method utilized did not provide information for the complete fraction, but only during the first treatment arc. Furthermore, the intrafraction data recorded was averaged during the 2–3 DIBHs needed to deliver the first treatment arc. This effect might slightly deteriorate CBCT image quality compared to a CBCT acquisition in one DIBH. In this regard, DIBH CBCTs image quality was still superior to free-breathing CBCTs, even considering the imperfect DIBH reproducibility [12].

The election of the registration method utilized implied two limitations. On one side, we were not able to distinguish whether a measured shift was due to a tumor shift relative to bony anatomy (pure tumor shift) or due to a shift of the whole patient. On the other side, the coherence in the registration between a CT and a CBCT is not perfect, therefore introducing new uncertainties. However, we decided to use the planning CT as the reference image, thus registering both the setup and the intrafraction CBCTs to it. This study was performed retrospectively and all shifts were acquired using the usual clinical workflows, which implies considering the planning CT as the reference image. Furthermore, if we had decided to register the intrafraction CBCT with a pre-treatment CBCT we would have needed to perform an extra CBCT immediately after the corrections were applied. This would have increased the number of images needed, therefore increasing the dose received by the patients.

With regard to the clinical importance of our study, we lack enough data to state which system is clinically superior for DIBH lung SBRT treatments. Although we have found statistically significant differences in our results, the clinical relevance associated to using one system or the other might be negligible. Further investigation should be performed so as to elucidate whether differences obtained are clinically relevant or not.

In this study, the intrafraction shift in 157 lung SBRT patients was addressed when using two distinct systems to perform DIBH. SB and SG can be considered as accuracy-equivalent systems. However, SB was more precise than SG. Lesion location influenced intrafraction motion as inferior lobe lesions offsets were larger in SI and superior lobe lesions offsets were higher in AP. Further efforts should be made to quantify and isolate possible sources of intrafraction motion in lung tumors and find mechanisms to overcome them.

## Declaration of Competing Interest

The authors declare that they have no known competing financial interests or personal relationships that could have appeared to influence the work reported in this paper.

## References

[1] Benedict SH, Yenice KM, Followill D, Galvin JM, Hinson W, Kavanagh B, et al. Stereotactic body radiation therapy: the report of AAPM Task Group 101. Med Phys 2010;37:4078–101. https://doi.org/10.1118/1.3438081.

[2] Vergalasova I, Cai J. A modern review of the uncertainties in volumetric imaging of respiratory-induced target motion in lung radiotherapy. Med Phys 2020;47: e988–1008. https://doi.org/10.1002/mp.14312.
[3] van Herk M. Errors and margins in radiotherapy. Semin Radiat Oncol 2004;14: 52–64. https://doi.org/10.1053/j.semradonc.2003.10.003.
[4] Stephans KL, Djemil T, Tendulkar RD, Robinson CG, Reddy CA, Videtic GM. Prediction of chest wall toxicity from lung stereotactic body radiotherapy (SBRT). Int J Radiat Oncol Biol Phys 2012;82:974–80. https://doi.org/10.1016/j.ijrobp.2010.12.002.
[5] Ong CL, Palma D, Verbakel WF, Slotman BJ, Senan S. Treatment of large stage I-II lung tumors using stereotactic body radiotherapy (SBRT): planning considerations and early toxicity. Radiother Oncol 2010;97:431–6. https://doi.org/10.1016/j.radonc.2010.10.003.
[6] Bouilhol G, Ayadi M, Rit S, Thengumpallil S, Schaerer J, Vandemeulebroucke J, et al. Is abdominal compression useful in lung stereotactic body radiation therapy? a 4DCT and dosimetric lobe-dependent study. Phys Med 2013;29:333–40. https://doi.org/10.1016/j.ejmp.2012.04.006.
[7] Dumas M, Laugeman E, Sevak P, Snyder KC, Mao W, Chetty IJ, et al. Technical Note: comparison of the internal target volume (ITV) contours and dose calculations on 4DCT, average CBCT, and 4DCBCT imaging for lung stereotactic body radiation therapy (SBRT). J Appl Clin Med Phys 2020;21:288–94. https://doi.org/10.1002/acm2.13041.
[8] Boda-Heggemann J, Knopf AC, Simeonova A, Wertz H, Stieler F, Jahnke A, et al. DIBH (Deep Inspiratory Breath Hold)-based radiotherapy – a clinical review. Int J Radiat Oncol Biol Phys 2015;94:478–92. https://doi.org/10.1016/j.ijrobp.2015.11.049.
[9] Wong VY, Tung SY, Ng AW, Li FA, Leung JO. Real-time monitoring and control on deep inspiration breath-hold for lung cancer radiotherapy: combination of ABC and external marker tracking. Med Phys 2010;37:4673–83. https://doi.org/10.1118/1.3476463.
[10] Bertholet J, Knopf A, Eiben B, McClelland J, Grimwood A, Harris E et al. Real-time intrafraction motion monitoring in external beam radiotherapy. Phys Med Biol. 2019;7;64. https://doi.org/10.1088/1361-6560/ab2ba8.
[11] Panakis N, McNair HA, Christian JA, Mendes R, Symonds-Tayler JR, Knowles C, et al. Defining the margins in the radical radiotherapy of non-small cell lung cancer (NSCLC) with active breathing control (ABC) and the effect on physical lung parameters. Radiother Oncol 2008;87:65–73. https://doi.org/10.1016/j.radonc.2007.12.012.
[12] Josipovic M, Persson GF, Bangsgaard JP, Specht L, Aznar MC. Deep inspiration breath-hold radiotherapy for lung cancer: impact on image quality and registration uncertainty in cone beam CT image guidance. Br J Radiol 2016;89:1068. https://doi.org/10.1259/bjr.20160544.
[13] Josipovic M, Aznar MC, Thomsen JB, Scherman J, Damkjaer SM, Nygård L et al. Deep inspiration breath hold in locally advanced lung cancer radiotherapy: validation of intrafractional geometric uncertainties in the INHALE trial. Br J Radiol 2019;92:1104. https://doi.org/10.1259/bjr.20190569.
[14] Wong JW, Sharpe MB, Jaffray DA, Kini VR, Robertson JM, Stromberg JS, et al. The use of active breathing control (ABC) to reduce margin for breathing motion. Int J Radiat Oncol Biol Phys 1999;44:911–9. https://doi.org/10.1016/s0360-3016(99)00056-5.
[15] Josipovic M, Persson GF, Dueck J, Bangsgaard JP, Westman G, Specht L et al. Geometric uncertainties in voluntary deep inspiration breath hold radiotherapy for locally advanced lung cancer. Radiother Oncol. 2016;118:510–514. https://doi.org/101016/jradonc201511004.
[16] Wang X, Zhong R, Bai S, Xu Q, Zhao Y, Wang J, et al. Lung tumor reproducibility with active breath control (ABC) in image-guided radiotherapy based on cone-beam computed tomography with two registration methods. Radiother Oncol 2011;99:148–54. https://doi.org/10.1016/j.radonc.2011.05.020.
[17] Cheung PC, Sixel KE, Tirona R, Ung YC. Reproducibility of lung tumor position and reduction of lung mass within the planning target volume using active breathing control (ABC). Int J Radiat Oncol Biol Phys 2003;57:1437–42. https://doi.org/10.1016/j.ijrobp.2003.08.006.
[18] Shi C, Tang X, Chan M. Evaluation of the new respiratory gating system. Precis Radiat Oncol 2017;1:127–33. https://doi.org/10.1002/pro6.34.
[19] Naumann P, Batista V, Farnia B, Fischer J, Liermann J, Tonndorf-Martini E, et al. Feasibility of optical surface-guidance for position verification and monitoring of stereotactic body radiotherapy in deep-inspiration breath-hold. Front Oncol 2020; 10:573279. https://doi.org/10.3389/fonc.2020.573279.
[20] Li R, Han B, Meng B, Maxim PG, Xing L, Koong AC, et al. Clinical implementation of intrafraction cone beam computed tomography imaging during lung tumor stereotactic ablative radiation therapy. Int J Radiat Oncol Biol Phys 2013;87: 917–23. https://doi.org/10.1016/j.ijrobp.2013.08.015.
[21] Caillet V, Booth JT, Keall P. IGRT and motion management during lung SBRT delivery. Phys Med 2017;44:113–22. https://doi.org/10.1016/j.ejmp.2017.06.006.
[22] Ottosson W, Rahma F, Sjöström D, Behrens CF, Sibolt P. The advantage of deep-inspiration breath-hold and cone-beam CT based soft-tissue registration for locally advanced lung cancer radiotherapy. Radiother Oncol 2016;119:432–7. https://doi.org/10.1016/j.radonc.2016.03.012.
[23] Graadal J, Ramberg C, Skar B, Paulsen T. Intrafractional motion in stereotactic body radiotherapy of spinal metastases utilizing cone beam computed tomography image guidance. Phys Imaging Radiat Oncol 2019;12:1–6. https://doi.org/10.1016/j.phro.2019.10.001.
[24] Hazelaar C, Dahele M, Scheib S, Slotman BJ, Verbakel W. Verifying tumor position during stereotactic body radiation therapy delivery using (limited-arc) cone beam computed tomography imaging. Radiother Oncol 2017;123:355–62. https://doi.org/10.1016/j.radonc.2017.04.022.
[25] Seppenwoolde Y, Shirato H, Kitamura K, Shimizu S, van Herk M, Lebesque JV, et al. Precise and real-time measurement of 3D tumor motion in lung due to breathing and heartbeat, measured during radiotherapy. Int J Radiat Oncol Biol Phys 2002;53:822–34. https://doi.org/10.1016/s0360-3016(02)02803-1.
[26] Chen T, Qin S, Xu X, Jabbour SK, Haffty BG and Yue NJ. Frequency filtering based analysis on the cardiac induced lung tumor motion and its impact on the radiotherapy management. Radiother Oncol. 2014;112:365–370. https://doi.org/101016/jradonc201408007.
[27] Kimura T, Murakami Y, Kenjo M, Kaneyasu Y, Wadasaki K, Ito K, et al. Interbreath-hold reproducibility of lung tumour position and reduction of the internal target volume using a voluntary breath-hold method with spirometer during stereotactic radiotherapy for lung tumours. Br J Radiol 2007;80:355–61. https://doi.org/10.1259/bjr/31008031.
[28] Keall PJ, Mageras GS, Balter JM, Emery RS, Forster KM, Jiang SB, et al. The management of respiratory motion in radiation oncology report of AAPM Task Group 76. Med Phys 2006;33:3874–900. https://doi.org/10.1118/1.2349696.
[29] Lu L, Diaconu C, Djemil T, Videtic GM, Abdel-Wahab M, Yu N, et al. Intra- and inter-fractional liver and lung tumor motions treated with SBRT under active breathing control. J Appl Clin Med Phys 2018;19:39–45. https://doi.org/10.1002/acm2.12220.
[30] den Otter LA, Kaza E, Kierkels RGJ, Meijers A, Ubbels FJF, Leach MO, et al. Reproducibility of the lung anatomy under active breathing coordinator control: dosimetric consequences for scanned proton treatments. Med Phys 2018;45: 5525–34. https://doi.org/10.1002/mp.13195.
[31] Scherman Rydhög J, Riisgaard de Blanck S, Josipovic M, Irming Jølck R, Larsen KR, Clementsen P, et al. Target position uncertainty during visually guided deep-inspiration breath-hold radiotherapy in locally advanced lung cancer. Radiother Oncol 2017;123:78–84. https://doi.org/10.1016/j.radonc.2017.02.003.
[32] Garibaldi C, Catalano G, Baroni G, Tagaste B, Riboldi M, Spadea MF, et al. Deep inspiration breath-hold technique guided by an opto- electronic system for extracranial stereotactic treatments. J Appl Clin Med Phys 2013;14:4087. https://doi.org/10.1120/jacmp.v14i4.4087.
[33] Peng Y, Vedam S, Chang JY, Gao S, Sadagopan R, Bues M, et al. Implementation of feedback-guided voluntary breath-hold gating for cone beam CT-based stereotactic body radiotherapy. Int J Radiat Oncol Biol Phys 2011;80:909–17. https://doi.org/10.1016/j.ijrobp.2010.08.011.